Ther Adv Ophthalmol
2020, Vol. 12: 1–8
DOI: 10.1177/2515841420922740

In vivo optical biopsy of choroidal osteoma: a swept source optical coherence tomography–based tumor characterization

Shorya Vardhan Azad, Vinod Kumar, Rohan Chawla, Bibhuti Kashyap, Shreyas Temkar, Atul Kumar, Pradeep Venkatesh, Rajpal Vohra, Kabiruddin Molla and Anu Sharma

Abstract

Objective: To study tumor characteristics of choroidal osteoma by swept source optical coherence tomography.

Methods: A retrospective case series done at tertiary referral center in northern India. All patients diagnosed with choroidal osteoma examined on swept source optical coherence tomography were included. Swept source optical coherence tomography images were analyzed for integrity of retinal layers—intraretinal layers, outer retinal layers (photoreceptor), retinal pigment epithelium, and contour abnormalities. Choroidal changes assessed were tumor attributes such as shape, depth of choroidal involvement, tumor mass reflectivity pattern, tumor vascularity, and evolutionary structural abnormalities such as deossification, focal depressions, or choroidal neovascular membrane.

Results: A total of 15 eyes of 11 patients were analyzed. Seven of 11 patients were females. Mean age of presentation was approximately 26 years. Tumor was large in nine cases (>7.5 mm). Deossification was seen in 12 eyes. Inner and outer retinal integrity was maintained in 7 and 2 eyes, respectively. Most common internal tumor reflectivity pattern seen was a lamellar appearance (12/15). Increased signal transmission to choroid and focal area of deep excavation was present in 11 and 4 eyes, respectively. Osteoclastic activity was noted in 12 eyes. Choroidal neovascular membrane was seen in 6 eyes. Small lesions showed lamellar pattern of tumor reflectivity with preservation of retinal pigment epithelium and overlying retina. Larger tumors were deossified with 6 irregular tumor contour, disorganization of the outer retina, increased signal transmission to choroid, and areas of osteoclastic activity.

Conclusion: Swept source optical coherence tomography was helpful in assessing tumor attributes and predicting the different timelines in tumor evolution.

Keywords: choroidal osteoma, choroidal neovascular membrane osteoma, deossified choroidal osteoma, swept source optical coherence tomography

Received: 5 September 2019; revised manuscript accepted: 2 March 2020.

Correspondence to:
Rohan Chawla
Dr. Rajendra Prasad Centre for Ophthalmic Sciences, AIIMS, New Delhi 110029, India
dr.rohanrpc@gmail.com

Shorya Vardhan Azad
Vinod Kumar
Bibhuti Kashyap
Shreyas Temkar
Atul Kumar
Pradeep Venkatesh
Rajpal Vohra
Kabiruddin Molla
Anu Sharma
Dr. Rajendra Prasad Centre for Ophthalmic Sciences, AIIMS, New Delhi, India

Introduction

Choroidal osteoma (CO) is a benign ossifying tumor of the choroid.[1] It is mostly unilateral and affects young women who may remain asymptomatic until development of a complication during tumor evolution.[2] Classically, fundus reveals an orange yellow, slightly elevated lesion, located near the disk or at the macula.[3] The diagnosis of CO is clinical and may be aided by ultrasonography. Tumor characteristics such as location, size, evolution, and complications have been described thus far by clinical examination, optical coherence tomography (OCT) and occasionally by histopathology.[3,4] Rarity of these lesions and absence of in vitro analysis studies are major hurdles in our understanding of this tumor.

Initially, only clinical clues such as tumor color had helped us differentiate between ossified and deossified areas.[5] This soon changed with the advent of OCT, by which histological correlation of different retinal and choroidal layers became possible. However, earlier OCT platform, the time-domain optical coherence tomography (TD-OCT), had lesser number of scans/second and poor depth penetration resulting in low-resolution images, incapacitating us to view beyond the retinal pigment epithelium (RPE).[6,7] It improved considerably with spectral-domain optical coherence tomography (SD-OCT) with better resolution and near histological delineation of various layers of retina and choroid.[8] Furthermore, with enhanced depth imaging (EDI), choroidal imaging reached a new level with clear demarcation of different choroidal layers.[9] Presently swept source optical coherence tomography (SS-OCT), owing to its ultra-high resolution (3 μm), better penetration because of longer wavelength (1050 nm), and lesser loss of signal strength with increasing depth has helped us understand subtle imaging characteristics of choroidal pathologies at par with histological sections.[10]

SS-OCT has been used widely for the characterization of various choroidal tumors. Its use in CO is however limited.[11,12] The purpose of this study is to report SS-OCT imaging characteristics of CO in a large series of patients.

Methods

This is a retrospective study of consecutive patients with CO who presented with decreased visual acuity or was detected on routine examination. The study conformed to the tenets of declaration of Helsinki and ethics approval was provided by the institute ethics committee, All India Institute of Medical Sciences (AIIMS) (IECPG-119/26.04.17, RT-20/28.09.17). Informed consent was obtained from all the patients. We reviewed records of all patients diagnosed as CO at our tertiary eye care center in northern India during the period 1 January 2016 to 31 July 2017. Eleven patients diagnosed with CO examined on SS-OCT were included. All patients underwent systemic and ophthalmic examination inclusive of visual acuity, intraocular pressure (IOP), slit lamp examination, fundus examination, and ultrasound B-scans (USG). Diagnosis of CO was made clinically by the presence of an orange yellow or yellowish white, slightly elevated subretinal lesion, which was peripapillary or macular in location. The diagnosis was confirmed on USG as a highly reflective choroidal mass, which casted a shadow on underlying structures and persisted at lower gain.

All eyes underwent color fundus photographs, short-wave autofluorescence, and SS-OCT (DRI OCT-1; Topcon, Tokyo, Japan). With disk diameter (1.5 mm) as a reference, CO were classified as small (<3 DD), medium (>3 DD to <5 DD) and large (>5 DD) according to its greatest linear dimension. SS-OCT has a wavelength tunable laser centered at 1050 nm and tissue imaging depth of 2.6 mm. All images were separately evaluated by three observers (R.C., V.K., and S.V.A.). SS-OCT images of all patients were analyzed for integrity of retinal layers – inner retinal layers, outer retinal layers (photoreceptor), RPE, and contour abnormalities. Choroidal integrity was also assessed for tumor attributes such as shape, depth choroidal involvement, tumor mass reflectivity pattern, tumor vascularity, and evolutionary structural abnormalities such as deossification, focal depressions or choroidal neovascular membrane (CNVM). Tumor reflectivity was classified as either lamellar (hyperreflective lines interspersed with hyporeflective lines with a diffuse granular hyperintense-reflective appearance) or Spongy (hyporeflective spaces with hyperreflective dots) pattern. Hyporeflective spaces without hyperreflective dots were noted as areas of presumed osteoclastic activity.

Results

A total of 15 eyes of 11 patients were analyzed. Seven of 11 patients were females, four had bilateral involvement. Mean age of presentation was 26.43 (16–40) years. All eyes had a single lesion with three being small (<3 DD), three medium (>3 DD to <5 DD), and nine large (>5 DD). Areas of deossification seen as yellowish whitish discoloration were present in all medium and larger lesions (12/12) (Figure 1(a)). These areas were more central in location with relative sparing of the periphery. Translucent areas were seen within the deossified portions leading to blurring of underlying tumor (Figure 2(a)). This translucent area indicated a focal excavation within the lesion, present in four cases. Intra/subretinal hemorrhages present at or near the fovea were noted in three cases (Table 1).

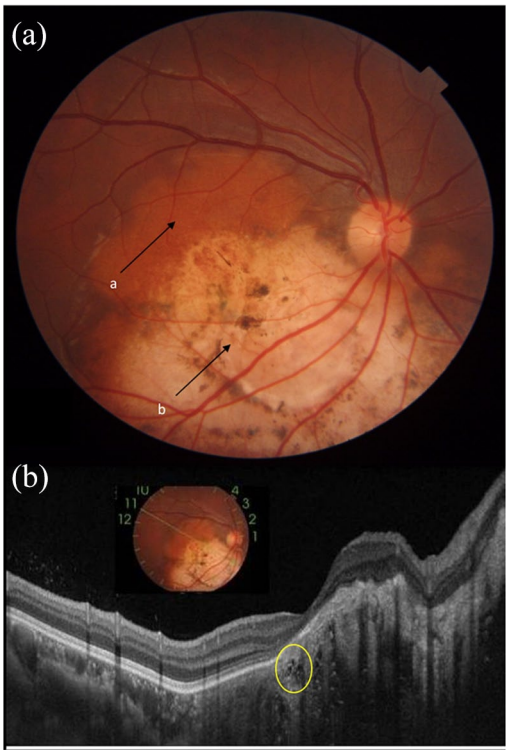

Figure 1. (a) Choroidal osteoma with: a indicates the orange looking ossified area and b indicates pale yellow deossified area. (b) Swept source optical coherence tomography showing focal osteoclastic activity between ossified and deossified area (yellow circle).

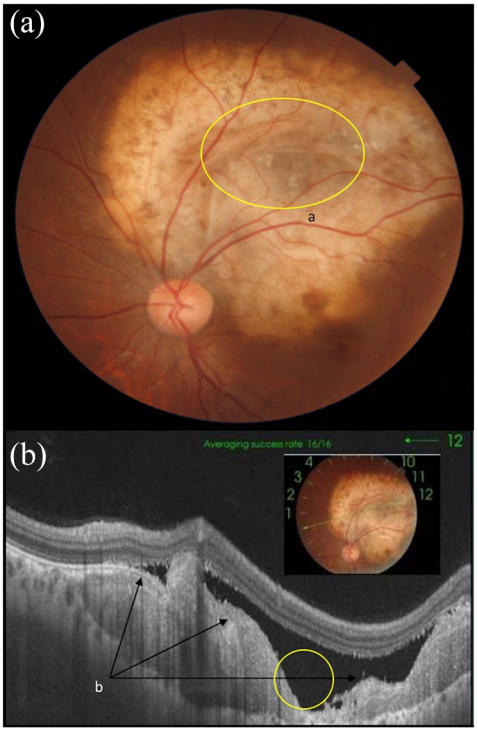

Figure 2. (a) Morphologically translucent area of choroidal osteoma (yellow circle). (b) Irregular surface contour of the tumor on swept source optical coherence tomography. (c) Focal excavation (yellow circle).

According to lesion size, small lesions showed no area of deossification (3/3). On SS-OCT, they had normal inner and outer retinal layers (3/3), convex tumor surface (3/3) and lamellar internal reflectivity (3/3). Medium lesions had a deossified area covering more than 50% of the lesion (2/3) (Figure 3(a)). SS-OCT revealed, lamellar internal reflectivity (3/3) and presumed osteoclastic activity (3/3) with inner retinal layers showing cystic spaces (2/3) and intraretinal fluid (2/3) eyes (Figure 3(b)). Outer retinal layers showed loss of photoreceptors along with RPE in all (3/3), choroidal neovascular membrane was seen in (2/3) with irregular tumor contour (3/3). Larger lesions had deossified area greater than 50% in all but two eye (7/9) (Figures 1(a), 2(a) and 3(a)). On SS-OCT, cystic spaces (4/9) with intraretinal fluid (3/9) in inner retinal layers was noted. Outer retinal layers showed photoreceptor loss along with RPE atrophy in all (9/9), CNVM was seen in (4/9), irregular tumor contour (8/9), lamellar internal reflectivity (6/9), presumed osteoclastic activity (9/9), and focal excavation/trench formation was seen in (4/9) (Figure 2(b)) (Table 2).

Deossified tumors (Total: 12) were typically large (9/12) or moderate in size (3/12). Disruption of the outer retinal layers (12/12) was seen universally in the areas of deossification. In addition, these had an irregular contour (11/12) with greater area of possible osteoclastic activity (12/12). Likelihood of complications such as CNVM (6/12) and trench formation (4/12) also increased with greater deossification of tumor. Deossification was absent in small lesions (3/3). It was noted more centrally (3/3) in medium lesions (Figure 3(a)) and showed greater spread in larger lesions (9/9) (Figures 2(a) and 4(a)). Increased OCT signal transmission to choroid was seen in all lesions in areas of deossification (11/12) (Figure 4(a)).

Discussion

COs do undergo evolutionary changes during the course of their existence.[13–15] These changes may

Table 1. Clinical Features

S. No.	Sex	Size	Location	Deossification	Area of deossification	F.E.	Bleed at fovea
1	FEMALE	SMALL	MACULAR				
2	FEMALE	LARGE	S.B	+	>50%	+	+
3	FEMALE	SMALL	MACULAR				
4	FEMALE	MEDIUM	MACULAR	+	>50%		
5	FEMALE	LARGE	S.B	+	>50 %		
6	FEMALE	MEDIUM	ARCADES	+	<50%		
7	MALE	LARGE	A.A.D	+	<50%		+
8	MALE	SMALL	ARCADES				
9	FEMALE	LARGE	S.B	+	<50%		
10	FEMALE	LARGE	S.B	+	>50%	+	
11	FEMALE	LARGE	S.B	+	>50%		
12	MALE	LARGE	A.A.D	+	>50%	+	
13	FEMALE	LARGE	A.A.D	+	>50%	+	
14	MALE	MEDIUM	MACULAR	+	>50%		+
15	FEMALE	LARGE	I.B	+	>50%		
TOTAL				12		4	3

A.A.D., all around the disk; F.E., focal excavation; I.B., inferior border of disk; S.B., superior border of disk.

have an eventual bearing on the visual acuity.[12] To date, histology is the best the technique for studying tumor characteristics; however, OCT is nearly as good, although its resolution and depth of penetration thus far have been its limitation.[16] Newer SS-OCT platform has overcome these limitations to give us ultra-high resolution images, delineating all retinal and choroidal layers.[10] Recent study by Shields et al,[9] described OCT features of CO with the help of EDI, giving us an insight into tumor morphology such as the presence of bone lamellae, cement lines, Haversian canals, Volkmann canals, and trabeculae. However, effect of aging on internal tumor reflectivity pattern and adjacent retinal/choroidal damage on SS-OCT had not been studied.

In our study, we divided lesions according to their size and the presence of deossification, the two main clinical clues in practice till now signifying tumor age.[17,18] On SS-OCT, small tumors did not occupy the entire choroid and spared the outer choroidal vessels and the overlying choriocapillaris. Similar findings have been described on histology in earlier studies.[1] Tumor substance showed a tightly packed granular reflectivity with few horizontal hyperreflective lamellae. As the tumor size increased to medium, deossification was seen in most cases. Tumor substance showed similar reflectivity pattern as small lesions with addition areas of presumed osteoclastic activity present at the junction of ossified and deossified area (Figure 1). In larger tumors, deossification was seen in all cases except one, covering most of the tumor area. SS-OCT revealed greater area of presumed osteoclastic activity, which would explain greater area of deossification in large lesions. Three cases showed hyporeflective areas with hypereflective dots, sign of spongy bone as described by previous studies.[19] However,

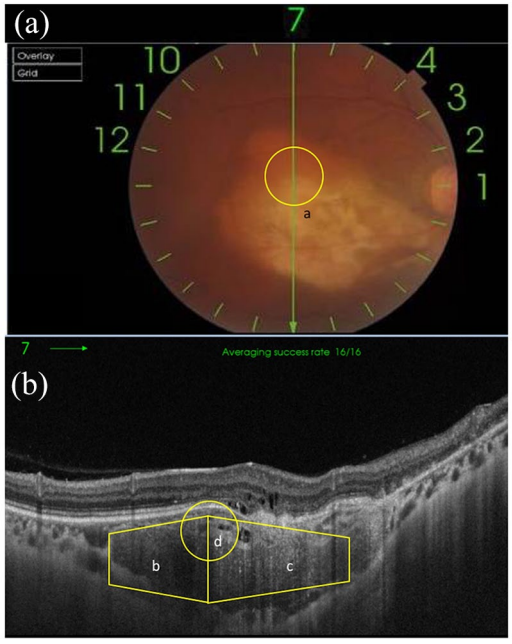

Figure 3. (a) Junction of ossified and deossified area of tumor on color photograph. (b) Swept source optical coherence tomography, b is the area of decreased signal transmission corresponding to ossified area of the tumor, c is the area of increased signal transmission corresponding to deossified area of the tumor, d is the junction between ossified and deossified area of the tumor corresponding to Figure 3(a).

granular hyperreflectivity with lamellae were more common than spongy pattern in our study, contrasting to what was observed in the aforementioned study.[19] Comparing these findings to the study by Shields et al, we were unable to characterize vertical and horizontal channels in the tumor, which they described as Haversian and Volkmann's cannals.[10] However, our study did echo similar tumor reflectivity patterns, with lamellar pattern being more common than the spongy pattern. We also identified areas of hyporeflectivity (hollow spaces) in the tumor body. They have been hypothesized in an earlier study to be area of bone remodeling. Therefore, its presence at the junction of ossified and deossified regions led us to propose them as sites of osteoclastic activity.

Second, in terms of deossification, it was absent in all smaller lesions and spread centrifugally (Figures 2(a), 3(a) and 4(a)) covering greater area as lesions grew larger, eventually leaving only the periphery in largest of lesions. In addition, there were peculiar translucent areas seen clinically, present within the deossified regions, with blurring of underlying tumor. These areas maybe sites of accelerated osteoclastic activity, leading to bone resorption and trench formation. They were confirmed on SS-OCT, as choroidal excavations due to loss of tumor tissue with dipping of the RPE and its approximation to the sclera (Figure 2). Numerous studies have noted such findings and tried to give possible explanations for it, labeling them as neurosensory detachment (NSD), focal choroidal excavation, and posterior staphyloma.[20–22] It is known that osteoclasts are found in pits on the bone surface which are called resorption bays, or Howship's lacunae; hence, the areas noted by us may be similar to Howship's lacunae indicating sites of osteoclastic activity.[23,24] All cases of deossification showed increased signal transmission to choroid owing to loss of RPE/photoreceptors, in areas of deossification, often outlining its entire boundary on OCT (Figure 3). We found increased choroidal transmission as a reliable marker of deossification on OCT just as altered fluorescence has been postulated on Fundus Autoflourescense (FAF) by previous studies (Figure 4).[17,18] Choroidal neovascular membrane was absent in ossified tumors (0/3), and chances of its presence grew with greater deossification (6/12). Its association with focal choroidal excavation in cases of CO has been hypothesized in an earlier study.[11] However, out of four cases of Focal Excavation (FE) in our study, only two had CNVM. CNVM appears to be of mixed variety. It appears over and above the altered fibrillary branching vasculature seen at the level of the tumor in most of our cases. It was difficult to comment on the exact type, as marked disorganization of the outer retinal/RPE lead to inability to segment the layers. Fifty percent of these CNVM's presented as hemorrhages near the fovea.

Thus lesions of smaller size, uniform granular tumor reflectivity with lamellar pattern and preservation of RPE and overlying retina, tend to have a better visual acuity. Any future therapeutic modalities should be aimed at this stage of the tumor. Large tumors span the entire choroid with sparing of larger choroidal vessels. Large tumors eventually deossify that starts from the center and spreads centrifugally. Deossification is shown by the presence of irregular tumor contour, disorganization of the outer retina/RPE, and increased OCT signal transmission to choroid and areas of osteoclastic activity leading to bone resorption. Advanced stages of deossification ends in the formations of resorption bays/ditches due to continuous bone

Table 2. Swept Source OCT findings

S. No.	Size	Inner retina					Outer retina					Choroid									
		Normal	Cystic spaces	Intra-retinal fluid	Loss of dist-inction	Foveal thinning	Normal	RPE loss	PR loss	NSD	ORT	Full thickness involvement	Increased signal trans-mission	CNVM	Configuration		Reflectivity			F.E
															Convex	Irregular	Lamellar	Spongy	Osteoclastic	
1.	SMALL	+					+					+			+		+			
2.	SMALL	+					+								+		+			
3.	SMALL	+					+								+		+			
	TOTAL	3					3	0	0	0		1			3	0	3		0	
4.	MEDIUM		+		+			+	+				+			+	+		+	
5.	MEDIUM			+				+	+	+			+	+		+	+		+	
6.	MEDIUM		+	+				+	+				+	+		+	+		+	
	TOTAL	0	2	2	1			3	3	1			3	2	0	3	3		3	
7.	LARGE	+						+	+	+	+	+	+	+		+	+		+	+
8.	LARGE	+						+	+				+			+	+		+	
9.	LARGE		+	+				+	+					+	+			+	+	
10.	LARGE			+	+			+	+				+	+		+		+	+	
11.	LARGE	+						+	+				+			+		+	+	+
12.	LARGE		+		+			+	+			+	+			+	+		+	
13.	LARGE	+						+	+				+			+	+		+	+
14.	LARGE		+	+	+			+	+	+	+		+	+		+	+		+	+
15.	LARGE		+			+		+	+				+			+	+		+	
	TOTAL	4	4	3	3	1	0	9	9	2	2	2	8	4	1	8	6	3	9	4
	GRAND TOTAL	7/15 (46.6%)	6/15 (40%)	5/15 (33.3%)	4/15 (26.6%)	4/15 (26.6%)	3/15 (20%)	12/15 (80%)	12/15 (80%)	3/15 (20%)	2/15 (13.3%)	3/15 (20%)	11/15 (73.3%)	6/15 (40%)	4/15 (26.6%)	11/15 (73.3%)	12/15 (80%)	3/15 (20%)	12/15 (80%)	4/15 (26.6%)

CNVM, choroidal neovascular membrane; F.E., focal excavation; NSD, neurosensory detachment; ORT, outer retinal tubulations; PR, photoreceptor; RPE, retinal pigment epithelium.

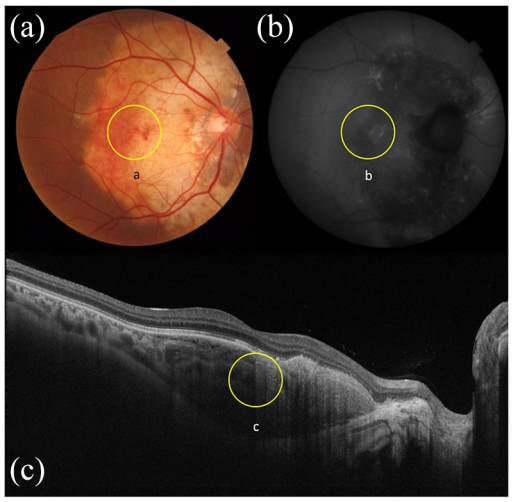

Figure 4. (a) Junction of ossified and deossified area, (b) on fundus autofluorescence as isoautofluorescent ossified area and hypoautofluorescent deossified area, and (c) corresponding junction on swept source optical coherence tomography.

remodeling and CNVM formation (as osteoclastic activity known to be linked to vascular endothelial growth factor (VEGF)).[25]

To conclude, SS-OCT is helpful in assessing tumor attributes and predicting the different timelines in tumor evolution.

Conflict of interest statement

The authors declared no potential conflicts of interest with respect to the research, authorship, and/or publication of this article.

Funding

The authors received no financial support for the research, authorship, and/or publication of this article.

ORCID iDs

Shorya Vardhan Azad https://orcid.org/0000-0002-8050-5812

Rohan Chawla https://orcid.org/0000-0002-6791-4435

References

1. Gass JD, Guerry RK, Jack RL, *et al.* Choroidal osteoma. *Arch Ophthalmol* 1978; 96: 428–435.
2. Aylward GW, Chang TS, Pautler SE, *et al.* A long-term follow-up of choroidal osteoma. *Arch Ophthalmol* 1998; 116: 1337–1341.
3. Shields CL, Shields JA and Augsburger J. Choroidal osteoma. *Survophthalmol* 1998; 33: 17–27.
4. Williams AT, Font RL, Van Dyk HJ, *et al.* Osseous choristoma of the choroid simulating a choroidal melanoma. Association with a positive 32P test. *Arch Ophthalmol* 1978; 96: 1874–1877.
5. Shields CL, Sun H, Demirci H, *et al.* Factors predictive of tumor growth, tumor decalcification, choroidal neovascularization, and visual outcome in 74 eyes with choroidal osteoma. *Arch Ophthalmol* 2005; 123: 1658–1666.
6. Shields CL, Perez B, Materin MA, *et al.* Optical coherence tomography of choroidal osteoma in 22 cases: evidence for photoreceptor atrophy over the decalcified portion of the tumor. *Ophthalmology* 2007; 114: e53–e58.
7. Ide T, Ohguro N, Hayashi A, *et al.* Optical coherence tomography patterns of choroidal osteoma. *Am J Ophthalmol* 2000; 130: 131–134.
8. Freton A and Finger PT. Spectral domain-optical coherence tomography analysis of choroidal osteoma. *Br J Ophthalmol* 2012; 96: 224–228.
9. Shields CL, Arepalli S, Atalay HT, *et al.* Enhanced depth imaging optical coherence tomography (EDI-OCT) of choroidal osteoma in 15 cases. *Retina* 2015; 35: 750–757.
10. Hayashia Y, Mitamuraa Y, Egawaa M, *et al.* Swept-source optical coherence tomographic findings of choroidal osteoma. *Case Rep Ophthalmol* 2014; 5: 195–202.
11. Pierro L, Marchese A, Gagliardi M, *et al.* Choroidal excavation in choroidal osteoma complicated by choroidal neovascularization. *Eye* 2017; 31: 1740–1743.
12. Azad SV, Takkar B, Venkatesh P, *et al.* Swept source: optical coherence tomography angiography features of choroidal osteoma with choroidal neovascular membrane. *BMJ Case Rep* 2016; 2016: bcr2016215899.
13. Shields JA, Shields CL, De Potter P, *et al.* Progressive enlargement of a choroidal osteoma. *Arch Ophthalmol* 1995; 113: 819–820.
14. Buettner H. Spontaneous involution of a choroidal osteoma. *Arch Ophthalmol* 1990; 108: 1517–1518.
15. Trimble SN and Schatz H. Decalcification of a choroidal osteoma. *Br J Ophthalmol* 1991; 75: 61–63.
16. Fukasawa A and Iijima H. Optical coherence tomography of choroidal osteoma. *Am J Ophthalmol* 2002; 133: 419–421.

17. Sisk RA, Riemann CD, Petersen MR, *et al*. Fundus autofluorescence findings of choroidal osteoma. *Retina* 2013; 33: 97–104.

18. Erol MK, Coban DT, Ceran BB, *et al*. Enhanced depth imaging optical coherence tomography and fundus autofluorescence findings in bilateral choroidal osteoma: a case report. *Arq Bras Oftalmol* 2013; 76: 189–191.

19. Navajas EV, Costa RA, Calucci D, *et al*. Multimodal fundus imaging in choroidal osteoma. *Am J Ophthalmol* 2012; 153: 890. e3–895.e3.

20. Szelog J, Bonini Filho MA, Lally DR, *et al*. Optical coherence tomography angiography for detecting choroidal neovascularization secondary to choroidal osteoma. *Ophthalmic Surg Lasers Imaging Retina* 2016; 47: 69–72.

21. Fung AT. Enhanced depth imaging-optical coherence tomography of choroidal osteoma. *JAMA Ophthalmol* 2015; 133: e143487.

22. Cheng YC, Shen JH, Chao AN, *et al*. Later development of posterior staphyloma in choroidal osteoma with choroidal neovascularization. *Retina* 2017; 37: e95–e96.

23. Kaye M. When is it an osteoclast? *J Clin Pathol* 1984; 37: 398–400.

24. Sedlin ED, Villanueva AR and Frost HM. Age variations in the specific surface of howship's lacunae as an index of human bone resorption. *Anat Rec* 1963; 146: 201–207.

25. Liu Y, Berendsen AD, Jia S, *et al*. Intracellular VEGF regulates the balance between osteoblast and adipocyte differentiation. *J Clin Invest* 2012; 122: 3101–3113.